Ma et al. Nanoscale Research Letters (2016) 11:170
DOI 10.1186/s11671-016-1390-0

Nanoscale Research Letters

NANO EXPRESS Open Access

Pinhole Effect on the Melting Behavior of $Ag@Al_2O_3$ SERS Substrates

Lingwei Ma[1], Yu Huang[1], Mengjing Hou[1], Jianghao Li[1] and Zhengjun Zhang[2*]

Abstract

High-temperature surface-enhanced Raman scattering (SERS) sensing is significant for practical detections, and pinhole-containing (PC) metal@oxide structures possessing both enhanced thermal stability and superior SERS sensitivity are served as promising SERS sensors at extreme sensing conditions. Through tuning the Al_2O_3 precursors' exposure time during atomic layer deposition (ALD), Al_2O_3 shells with different amount of pinholes were covered over Ag nanorods (Ag NRs). By virtue of these unique PC $Ag@Al_2O_3$ nanostructures, herein we provide an excellent platform to investigate the relationship between the pinhole rate of Al_2O_3 shells and the melting behavior, high-temperature SERS performances of these core-shell nanostructures. Pinhole effect on the melting procedures of PC $Ag@Al_2O_3$ substrates was characterized in situ via their reflectivity variations during heating, and the specific melting point was quantitatively estimated. It is found that the melting point of PC $Ag@Al_2O_3$ raised along with the decrement of pinhole rate, and substrates with less pinholes exhibited better thermal stability but sacrificed SERS efficiency. This work achieved highly reliable and precise control of the pinholes over Al_2O_3 shells, offering sensitive SERS substrates with intensified thermal stability and superior SERS performances at extreme sensing conditions.

Keywords: Metal@oxide nanostructures, Pinhole shell, Thermal stability, Melting point, SERS

Background

High-temperature surface-enhanced Raman scattering (SERS) detection is a vital part for practical sensing, which can be employed for monitoring many in situ reactions, e.g., thermal crystallization [1], structural variations [2, 3], and chemical reactions [4, 5] at elevated temperatures. However, bare metal nanostructures suffer from the inherently low melting point [6, 7], which causes the morphological instability of nano-sized metal and as a result, may deteriorate their SERS performances at high temperatures [2–4, 8–10]. Lately, core-shell nanostructures of metal core covered with protective oxide layer have been proposed as good SERS substrates for high-temperature Raman sensing [2, 3, 5, 8–10]. For example, wrapping Ag nanorods (Ag NRs) with an ultrathin (~1.5 nm) but dense Al_2O_3 layer could make the substrate robust in morphology at 400 °C and stabilize its SERS efficiency [10]. Most recently, novel metal@oxide structures with pinhole-containing (PC) shells have drawn tremendous attention, which could not only increase the working temperature of SERS substrates moderately [10], but also exhibited even better SERS properties and broader application fields compared with metal@oxide substrates of compact shells [11, 12]. Accordingly, it is highly desired to synthesize PC metal@oxide structures as ideal SERS-active substrates as well as investigate and optimize their properties.

However, up to now, the accurate control and measurements of the oxide pinhole rate, as well as the comprehensive investigation of the melting procedures and thermal stability of PC metal@oxide substrates, have not been investigated in detail. In this regard, herein we introduced atomic layer deposition (ALD) technique to cover Ag NRs with Al_2O_3 shells ($Ag@Al_2O_3$) of different pinhole amount and experimentally analyzed the Al_2O_3 pinholes' influence on the melting behavior of PC $Ag@Al_2O_3$ substrates. The pinholes can be readily tuned by varying the exposure time of Al_2O_3 precursors during ALD coating, and the pinhole rate was estimated using the Raman signals of acridine molecules on uncoated Ag NRs and PC $Ag@Al_2O_3$ substrates. The melting process of PC $Ag@Al_2O_3$ was monitored via their reflectivity

* Correspondence: zjzhang@tsinghua.edu.cn
[2]Key Laboratory of Advanced Materials (MOE), School of Materials Science and Engineering, Tsinghua University, Beijing 100084, People's Republic of China
Full list of author information is available at the end of the article

variations during heating, and the melting point of different substrates was quantitatively calculated and compared. In addition, the SERS performances of PC Ag@Al_2O_3 substrates were tested after thermal treatment, demonstrating excellent stability and versatility of these SERS sensors.

Methods

Fabrication of Ag NRs

Slanted Ag NRs were prepared on Si (001) substrates by oblique angle deposition (OAD) technique in an electron-beam system (GLAD, Thermionics Inc.) with a background vacuum level of 10^{-6} Pa. During deposition, the incident angle between the surface normal of substrates and vapor flux was set at ~86°, with a deposition rate of ~0.75 nm/s. The NR growth finished at a thickness of 1000 nm read by a quartz crystal microbalance [10, 12].

Fabrication of PC Ag@Al_2O_3 Substrates

Al_2O_3 layers were coated onto the as-prepared Ag NRs in an ALD reactor (MNT-100, Wuxi MNT Micro and Nanotech Co.) at 50 °C. The Al_2O_3 precursors, i.e., trimethylaluminum (TMA; maintained at 150 °C) and water (maintained at 40 °C), were alternatively pumped into the reaction chamber using high purity N_2 (99.999 %, 15 sccm) as the carrier and purge gas. In order to synthesize Al_2O_3 shells with a different pinhole rate, only one ALD cycle was used on top of Ag NRs and the exposure time of TMA and water was simultaneously changed during coating [10, 12]. One complete reaction consisted of four steps: (1) TMA reactant exposure, 2/5/10/20/40/80/100 ms; (2) N_2 gas purging, 10 s; (3) water vapor exposure, 1/2/5/10/20/40/50 ms; and (4) N_2 gas purging, 20 s. These substrates are denoted hereafter as Ag@Al_2O_3/2, Ag@Al_2O_3/5, Ag@Al_2O_3/10, Ag@Al_2O_3/20, Ag@Al_2O_3/40, Ag@Al_2O_3/80, and Ag@Al_2O_3/100, respectively. (These numbers represent the TMA exposure time during ALD coating)

Characterization of Ag NRs@Al_2O_3

The morphology and structures of Ag NRs and Al_2O_3 shells were characterized by scanning electron microscope (SEM; JEOL-JMS-7001F) and high-resolution transmission electron microscope (HRTEM; JEOL-2011). The melting process of these substrates was monitored in situ via their reflectivity variations upon annealing, using Optical Power Thermal Analyzer (OPA-1200).

SERS Detections

Acridine and 4-mercaptobenzoic acid (4-MBA) with different concentrations were dissolved into ethanol. SERS measurements were conducted by an optical fiber micro-Raman system (i-Raman Plus, B&W TEK Inc.). Before detection, all substrates were merged into different solutions for 1 h, washed thoroughly to remove the residual molecules, and dried naturally in air. Raman spectra were obtained using a 785-nm laser as the excitation source, with an excitation power of 150 mW and the data collection time of 10 s for each spectrum. For every sample, the spectrum was obtained by averaging the spectra obtained from five different areas of the SERS substrate.

Results and Discussion

Figure 1a, b shows typical top-view and side-view SEM images of Ag@Al_2O_3/10 substrate, from which one sees clearly that the slanted NRs are well-separated and ~700 nm in length. Figure 1c illustrates the HRTEM image of Ag@Al_2O_3/10 with a PC Al_2O_3 shell, which is sub-nanometer thick and uniformly wraps Ag NRs. To explore the relationship between the exposure time of ALD precursors and Al_2O_3 pinhole rate, we introduced acridine, a SERS probe molecule that can directly interact with Ag surface instead of Al_2O_3 layers [11–13]. If there are any pinholes in Al_2O_3 shells, acridine would adsorb on Ag surface through pinholes and exhibit Raman signals, paving a reliable way toward the characterization of Al_2O_3 pinholes. One sees from Fig. 1d that the Raman spectra of 1×10^{-2} M acridine molecules [14, 15] showed up not only on uncoated Ag NRs but also on PC Ag@Al_2O_3 substrates with distinct TMA/water exposure time, indicating that all these substrates had PC shells with exposed Ag surface inside. Because of the saturation of 1×10^{-2} M acridine over uncoated Ag NRs (see Additional file 1: Figure S1), we further utilized the acridine spectra from different substrates to estimate the pinhole rate of Al_2O_3 shells, via dividing acridine Raman intensity at 1403 cm^{-1} from PC Ag@Al_2O_3 substrates by that from uncoated Ag NRs. It is shown in Table 1 that the Al_2O_3 pinhole rate declined gradually with the increment of TMA/water exposure time, suggesting that longer exposure time provide better opportunity for TMA and water to react over Ag NRs. The pinhole rate ranges from ~18.0 to ~5.3 %, and further longer exposure time results in no obvious change of the pinhole rate.

Since optical property of nanostructures is sensitive to their morphology [16, 17], the melting procedures of PC Ag@Al_2O_3 substrates can be characterized in situ via their reflectivity changes upon annealing. Figure 2 thoroughly investigates the melting process and morphological changes of uncoated Ag NRs and Ag@Al_2O_3/10 at 50–350 °C (red line). Because melting occurs during a continuous process instead of at a specific point, to specifically and quantitatively characterize the melting point of different substrates, we define the extreme point of the reflectivity's derivative (blue line) from each sample as their melting point, at which temperature the morphology of nanostructures changes most dramatically [18, 19]. For bare Ag NRs, the reflectivity began to change at ~120 °C and the obvious shape variation was observed at 150 °C, which would affect the efficiency of SERS substrates. The

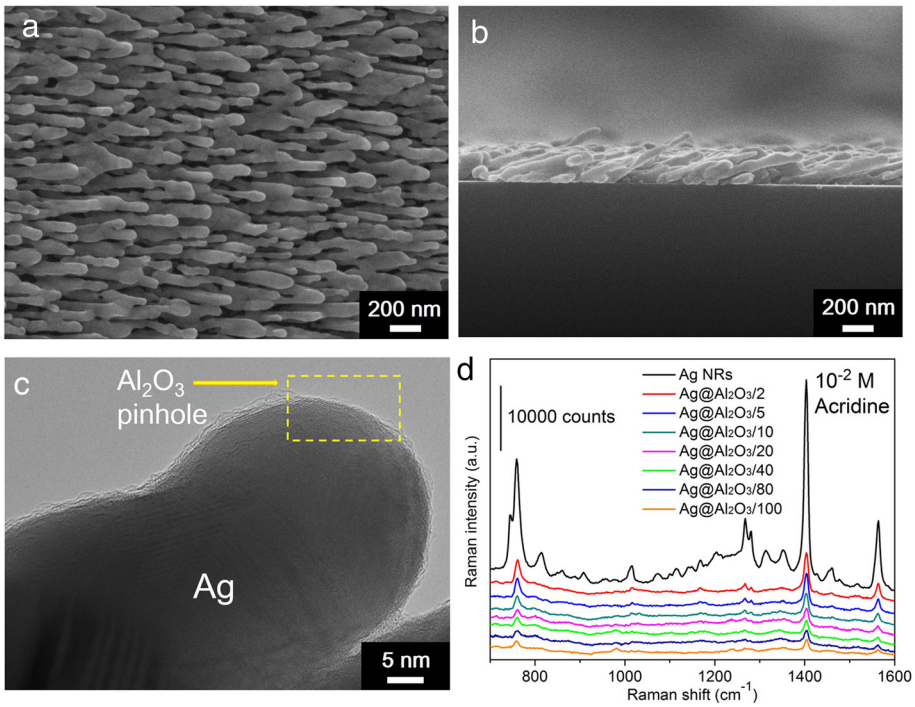

Fig. 1 **a** Typical top-view SEM, **b** side-view SEM, and **c** HRTEM images of Ag@Al_2O_3/10 substrate. **d** Raman spectra of 1×10^{-2} M acridine from uncoated Ag NRs and PC Ag@Al_2O_3 substrates with distinct TMA/water exposure time

structure distortion facilitated with increasing the annealing temperatures, and Ag NRs lost completely their shape after the melting point of ~197 °C, suggesting the instability nature of nano-sized Ag. As for Ag@Al_2O_3/10, the substrate maintained its shape at ~200 °C, and the melting point was as high as ~265 °C. It is particularly noted that although the morphology change of Ag@Al_2O_3/10 initiated at ~200 °C, the substrate kept partly the NR shape even at 350 °C, indicating the superior protection of Al_2O_3 shell. Figure 3 represents the SEM images of Ag@Al_2O_3/2, Ag@Al_2O_3/5, Ag@Al_2O_3/20, Ag@Al_2O_3/40, Ag@Al_2O_3/80, and Ag@Al_2O_3/100 after heating at 350 °C. It is observed that the substrates with less or smaller Al_2O_3 pinholes could keep better the nanorod shape and generate less fusion spots after annealing, indicating the pinhole rate's effect on the thermal and morphological stability of these substrates. Furthermore, the melting point of various PC Ag@Al_2O_3 substrates as a function of their pinhole rate was quantitatively evaluated and depicted in Fig. 4. Remarkably, we found that their melting point increase monotonously with the decrease of pinhole rate, starting from 257 °C with ~18.0 % pinholes and reaching a maximum at 277 °C when the pinhole rate was ~5.3 %. These results clearly demonstrate that the Al_2O_3 coverage provides a useful opportunity to strengthen the thermal stability of Ag nanostructures, which also offers us a means to precisely control the melting point of PC Ag@Al_2O_3 substrates.

Table 1 Pinhole rate of different PC Ag@Al_2O_3 substrates

Sample name	Pinhole rate (%)
Ag NRs	100
Ag@Al_2O_3/2	18.0
Ag@Al_2O_3/5	14.9
Ag@Al_2O_3/10	10.7
Ag@Al_2O_3/20	7.9
Ag@Al_2O_3/40	7.0
Ag@Al_2O_3/80	5.5
Ag@Al_2O_3/100	5.3

In the case of high-temperature SERS detection, 1×10^{-6} M 4-MBA [20, 21] was used to evaluate the SERS efficiency and thermal stability of PC Ag@Al_2O_3 substrates. Because SERS effect is highly localized and attenuates quickly away from metal surface [22, 23], a gradual decrement of 4-MBA Raman signals is observed with the decline of exposed Ag surface (see Fig. 5a). To be specific, the SERS intensity of 4-MBA on Ag@Al_2O_3/2, Ag@Al_2O_3/5, and Ag@Al_2O_3/10 with ~18.0 to ~10.7 % pinholes was about 80–70 % compared with that on uncoated Ag NRs. Further decrease of the pinhole rate led to a more dramatic drop of 4-MBA signals, which is consistent with the previous results of acridine molecules, except the fact that 4-MBA could interact not only with Ag surface but also with Al_2O_3 shells [24–27]. We should also mention that even though the SERS sensitivity of PC Ag@Al_2O_3 substrates

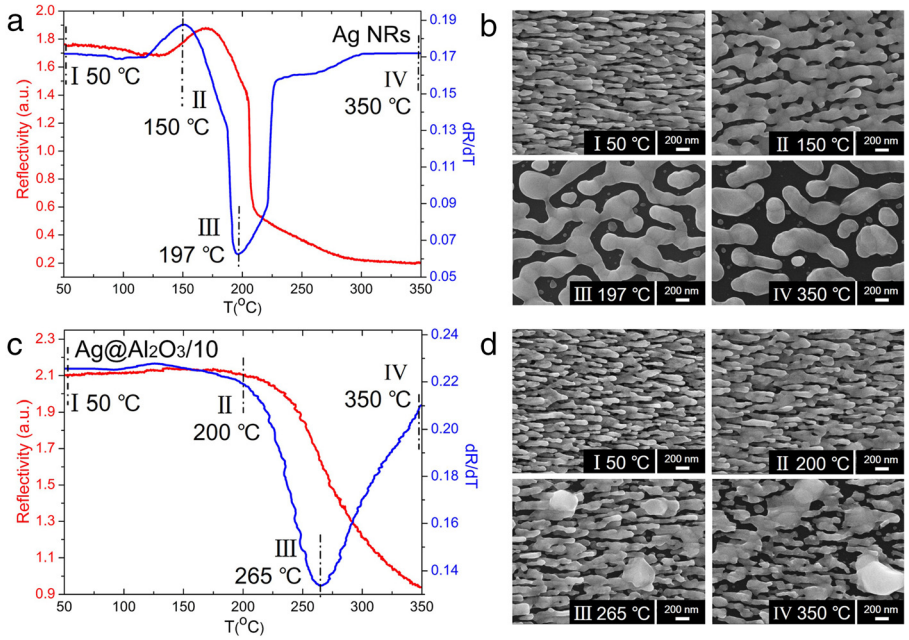

Fig. 2 The melting procedures of **a** uncoated Ag NRs and **c** Ag@Al_2O_3/10 at 50–350 °C through monitoring their reflectivity changes upon annealing (*red line*), and the corresponding extreme point of the reflectivity's derivative from each sample as their melting point (*blue line*). The morphological changes of **b** uncoated Ag NRs and **d** Ag@Al_2O_3/10 after heating

decreased to some extent after ALD coating, all these substrates with ultrathin Al_2O_3 shells and pinholes were highly effective for trace analyte recognition [12].

To demonstrate the feasibility of PC Ag@Al_2O_3 substrates for real-world applications, Ag@Al_2O_3/10 combined with both high melting point and good SERS activity was chosen to assess its high-temperature SERS performances, utilizing uncoated Ag NRs as a reference. It is observed from Fig. 5b that, when bare Ag NRs were heated at 200–350 °C, due to their significant morphological changes, the SERS activity decreased about one order of magnitude. On the contrary, although, at room temperature (RT), the SERS intensity of 4-MBA on Ag@Al_2O_3/10 was ~70 % in comparison with that on uncoated Ag NRs, this substrate was extremely robust in SERS performance at elevated temperatures. Approximately 5.5 times higher SERS enhancement was obtained from Ag@Al_2O_3/10 compared with that from bare Ag NRs when heated at 200 and 260 °C, indicating the strongly improved SERS stability of PC Ag@Al_2O_3 substrates. At 300 and 350 °C, Ag@Al_2O_3/10 showed moderate declines in SERS signals, which can be explained by its structure changes when exceeding its melting point of ~265 °C.

Conclusions

In summary, we successfully synthesized PC Ag@Al_2O_3 nanostructures with controllable pinhole rate and

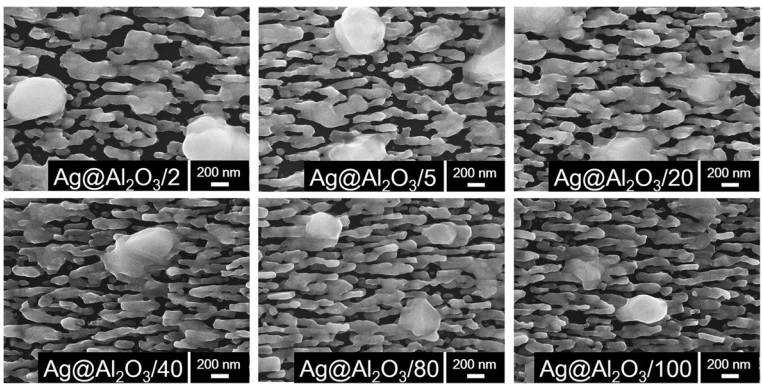

Fig. 3 SEM images of Ag@Al_2O_3/2, Ag@Al_2O_3/5, Ag@Al_2O_3/20, Ag@Al_2O_3/40, Ag@Al_2O_3/80, and Ag@Al_2O_3/100 after heating at 350 °C.

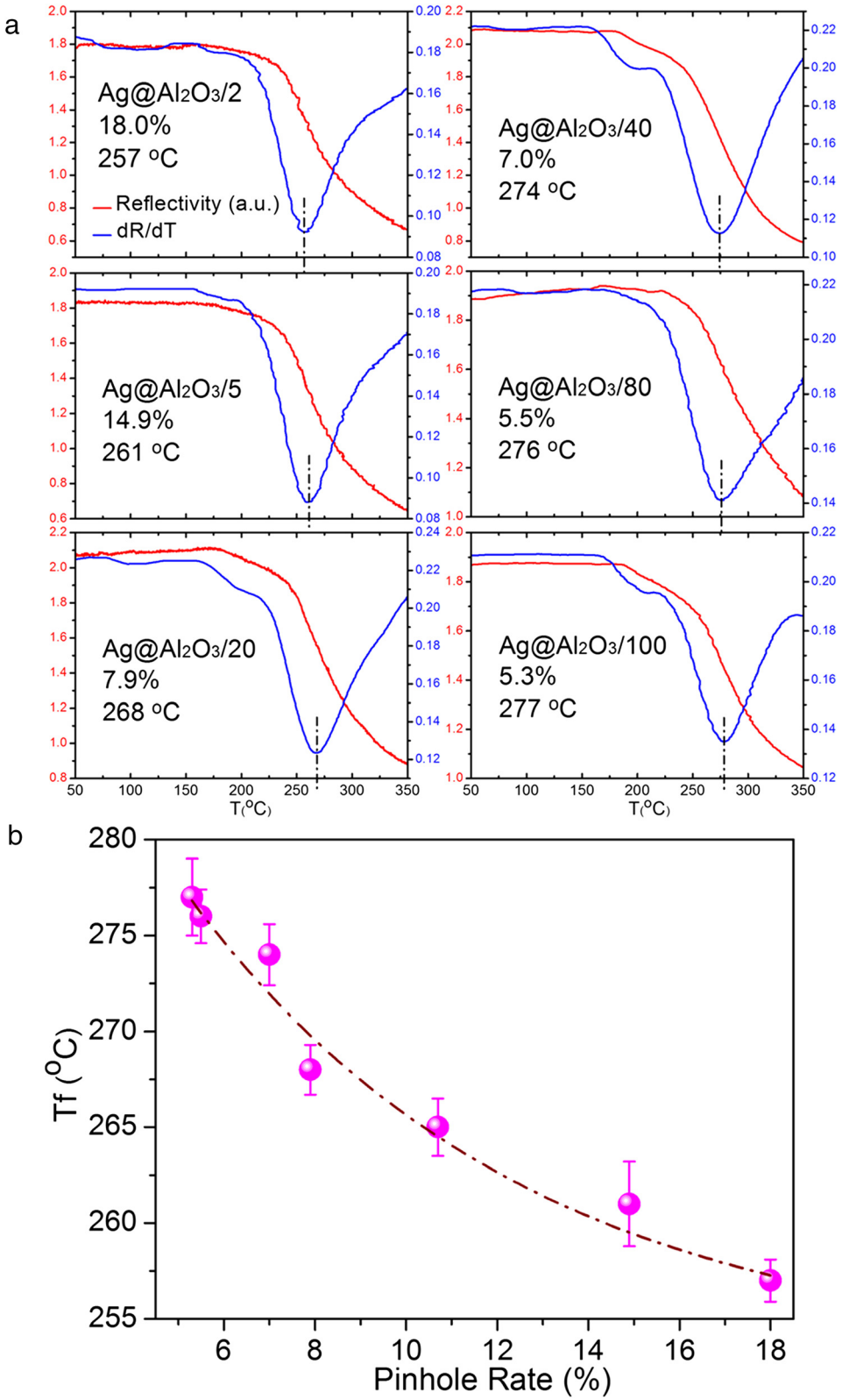

Fig. 4 **a** The melting procedures and the extreme point of the reflectivity's derivative from different PC Ag@Al_2O_3 substrates. **b** The melting point of PC Ag@Al_2O_3 substrates as a function of their pinhole rate

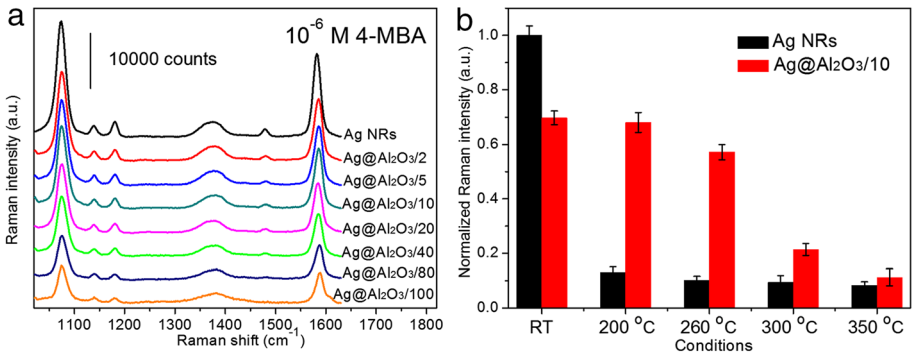

Fig. 5 a Typical Raman signals of 1×10^{-6} M 4-MBA molecules from uncoated Ag NRs and distinct PC Ag@Al_2O_3 substrates. **b** Normalized Raman intensity of 1×10^{-6} M 4-MBA from uncoated Ag NRs and Ag@Al_2O_3/10 at various conditions, i.e., at room temperature (RT), and after annealing at 200, 260, 300, and 350 °C, respectively.

investigated in detail the relationship between the melting behavior of PC substrates and Al_2O_3 pinhole rate. Due to the unique structures of these substrates, the melting point of PC Ag@Al_2O_3 increased along with the decline of the Al_2O_3 pinhole rate. By coating protective Al_2O_3 layers over Ag NRs, the substrates could preserve their structures and SERS efficiency at temperatures higher than 250 °C. These PC Ag@Al_2O_3 substrates with a controllable pinhole rate exhibit great potential as advanced platforms for high-temperature SERS detections.

Additional file

Additional file 1: Figure S1. Raman spectra of 1×10^{-1} M, 5×10^{-2} M, 1×10^{-2} M, and 1×10^{-3} M acridine molecules from uncoated Ag NRs. (DOCX 159 kb)

Abbreviations

4-MBA: 4-mercaptobenzoic acid; Ag NRs: Ag nanorods; ALD: atomic layer deposition; HRTEM: high-resolution transmission electron microscope; OAD: oblique angle deposition; PC: pinhole-containing; RT: room temperature; SEM: scanning electron microscope; SERS: surface-enhanced Raman scattering; TMA: trimethylaluminum.

Competing interests

The authors declare that they have no competing interests.

Authors' contributions

LM carried out the experiments. LM, YH, MH, JL, and ZZ participated in the design of the study. LM and ZZ conceived of the study and participated in its design and coordination and helped to draft the manuscript. All authors read and approved the final manuscript.

Authors' information

LM, YH, MH, and JL are PhD candidates at the School of Materials Science and Engineering, Tsinghua University.
ZZ is the head of the School of Materials Science and Engineering, Tsinghua University.

Acknowledgements

The authors are very grateful to the financial support by the National Basic Research Program of China (973 program, Grant No. 2013CB934301), the National Natural Science Foundation of China (Grant No. 51531006 and No. 51572148), the Research Project of Chinese Ministry of Education (Grant No. 113007A), and the Tsinghua University Initiative Scientific Research Program.

Author details

[1]State Key Laboratory of New Ceramics and Fine Processing, School of Materials Science and Engineering, Tsinghua University, Beijing 100084, People's Republic of China. [2]Key Laboratory of Advanced Materials (MOE), School of Materials Science and Engineering, Tsinghua University, Beijing 100084, People's Republic of China.

Received: 23 February 2016 Accepted: 22 March 2016
Published online: 31 March 2016

References

1. Muraki N (2014) In situ monitoring of thermal crystallization of ultrathin Tris (8-Hydroxyquinoline) aluminum films using surface-enhanced Raman scattering. Appl Spectrosc 68(1):39–43
2. Formo EV, Wu Z, Mahurin SM, Dai S (2011) In situ high temperature surface-enhanced Raman spectroscopy for the study of interface phenomena: Probing a solid acid on alumina. J Phys Chem C 115(18):9068–9073
3. Li X, Lee J, Blinn KS, Chen D, Yoo S, Kang B, Bottomley LA, El-Sayed MA, Park S, Liu M (2014) High-temperature surface-enhanced Raman spectroscopy for in situ study of solid oxide fuel cell materials. Energ Environ Sci 7(1):306–310
4. Liu M, Xiang R, Cao W, Zeng H, Su Y, Gui X, Wu T, Maruyama S, Tang Z (2014) Is it possible to enhance Raman scattering of single-walled carbon nanotubes by metal particles during chemical vapor deposition? Carbon 80: 311–317
5. John JF, Mahurin S, Dai S, Sepaniak MJ (2010) Use of atomic layer deposition to improve the stability of silver substrates for in situ, high-temperature SERS measurements. J Raman Spectrosc 41(1):4–11
6. Zhang Z, Su X, Zhao Y, Liu J, Pan C (2004) Characterization of Fe nanorods grown directly from submicron-sized iron grains by thermal evaporation. Phys Rev B 70(23):233404
7. Jiang Q, Zhang SH, Li JC (2004) Grain size-dependent diffusion activation energy in nanomaterials. Solid State Commun 130(9):581–584
8. Formo EV, Mahurin SM, Dai S (2010) Robust SERS substrates generated by coupling a bottom-up approach and atomic layer deposition. Acs Appl Mater Inter 2(7):1987–1991
9. Whitney AV, Elam JW, Stair PC, Van Duyne RP (2007) Toward a thermally robust operando surface-enhanced Raman spectroscopy substrate. J Phys Chem C 111(45):16827–16832
10. Ma L, Huang Y, Hou M, Xie Z, Zhang Z (2015) Silver nanorods wrapped with ultrathin Al_2O_3 layers exhibiting excellent SERS sensitivity and outstanding SERS stability. Sci Rep 5:12890
11. Gao J, Guo L, Wu J, Feng J, Wang S, Lai F, Xie J, Tian Z (2014) Simple and sensitive detection of cyanide using pinhole shell-isolated nanoparticle-enhanced Raman spectroscopy. J Raman Spectrosc 45(8):619–626
12. Ma L, Huang Y, Hou M, Li J, Xie Z, Zhang Z (2016) Pinhole-containing, subnanometer-thick Al_2O_3 shell-coated Ag nanorods as practical substrates for quantitative surface-enhanced Raman scattering. J Phys Chem C 120(1): 606–615

13. Uzayisenga V, Lin X, Li L, Anema JR, Yang Z, Huang Y, Lin H, Li S, Li J, Tian Z (2012) Synthesis, characterization, and 3D-FDTD simulation of Ag@SiO_2 nanoparticles for shell-isolated nanoparticle-enhanced Raman spectroscopy. Langmuir 28(24):9140–9146
14. Solovyeva EV, Myund LA, Dem Yanchuk EM, Makarov AA, Denisova AS (2013) Adsorption of acridine on silver electrode: SERS spectra potential dependence as a probe of adsorbate state. J Mol Struct 1034:19–21
15. Brayner R, Iglesias R, Truong S, Beji Z, Felidj N, Fiévet F, Aubard J (2010) Surface-enhanced Raman scattering on silver nanostructured films prepared by spray-deposition. Langmuir 26(22):17465–17469
16. Kelf TA, Baumberg JJ, Abdelsalam ME, Bartlett PN, Sugawara Y (2006) Strong coupling between localized plasmons and organic excitons in metal nanovoids. Phys Rev Lett 97(26):266808
17. Lindquist NC, Lesuffleur A, Oh S (2007) Lateral confinement of surface plasmons and polarization-dependent optical transmission using nanohole arrays with a surrounding rectangular Bragg resonator. Appl Phys Lett 91(25):253105
18. Tong H, Miao XS, Yang Z, Cheng XM (2011) Insulator-metal transition in GeTe/Sb_2Te_3 multilayer induced by grain growth and interface barrier. Appl Phys Lett 99(21):212105
19. Fang ZZ, Wang H (2008) Densification and grain growth during sintering of nanosized particles. Int Mater Rev 53(6):326–352
20. Jia P, Cao B, Wang J, Qu J, Liu Y, Pan K (2015) Self-assembly of various silver nanocrystals on PmPD/PAN nanofibers as a high-performance 3D SERS substrate. Analyst 140(16):5707–5715
21. Lin T, Wu H, Tasi T, Lai Y, Shen H (2015) Surface-enhanced Raman spectroscopy for DNA detection by the self-assembly of Ag nanoparticles onto Ag nanoparticle-graphene oxide nanocomposites. Phys Chem Chem Phys 17(28):18443–18448
22. Bai S, Li Q, Zhang H, Chen X, Luo S, Gong H, Yang Y, Zhao D, Qiu M (2015) Large third-order nonlinear refractive index coefficient based on gold nanoparticle aggregate films. Appl Phys Lett 107(14):141111
23. Zhou Z, Xue J, Zheng Z, Li J, Ke Y, Yu Y, Han J, Xie W, Deng S, Chen H, Wang X (2015) A centimeter-scale sub-10 nm gap plasmonic nanorod array film as a versatile platform for enhancing light-matter interactions. Nanoscale 7(37):15392–15403
24. Du P, Ma L, Cao Y, Li D, Liu Z, Wang Z, Sun Z (2014) Stable Ag@oxides nanoplates for surface-enhanced Raman spectroscopy of amino acids. Acs Appl Mater Inter 6(11):8853–8858
25. Zhang X, Zhao J, Whitney AV, Elam JW, Van Duyne RP (2006) Ultrastable substrates for surface-enhanced Raman spectroscopy: Al_2O_3 overlayers fabricated by atomic layer deposition yield improved anthrax biomarker detection. J Am Chem Soc 128(31):10304–10309
26. Nascimento FC, Carneiro CEA, Santana HD, Zaia DAM (2014) The effect of artificial seawater on SERS spectra of amino acids-Ag colloids: An experiment of prebiotic chemistry. Spectrochim Acta A 118:251–259
27. Tripathi A, Emmons ED, Christesen SD, Fountain AW III, Guicheteau JA (2013) Kinetics and reaction mechanisms of thiophenol adsorption on gold studied by surface-enhanced Raman spectroscopy. J Phys Chem C 117(44):22834–22842